The published version is available at: http://dx.doi.org/10.1109/TMAG.2012.2195190

Importance of Iron-Loss Modeling in Simulation of Wound-Field Synchronous Machines

Paavo Rasilo, Anouar Belahcen, Antero Arkkio

Aalto University School of Electrical Engineering
Department of Electrical Engineering, P.O. Box 13000, FI-00076 Aalto, Finland

Abstract—Effect of hysteresis, eddy-current and excess-loss modeling on the 2-D field solution of 12.5-MW and 150-kVA wound-field synchronous machines is studied. The study is performed by comparing the differences in the solutions obtained with three different finite element formulations: one with iron losses fully included, one using only single-valued material properties, and one completely neglecting the iron losses from the solution. The electrical operating points, i.e. the terminal currents and powers are found to be only little influenced by the iron-loss model. However, the rotor eddy-current losses are found to be overestimated, if the skin effect of the eddy currents is uncoupled from the solution. Using single-valued material properties instead of hysteretic ones has a smaller effect on the rotor side, but increases the hysteresis losses in the stator. The effects on the total core losses thus depend on their distribution between the stator and the rotor. It is concluded that using single-valued material properties is reasonable in order to improve the computational performance despite the slight overestimation in the computed core losses. However, for accurate modeling of the rotor losses, the skin effect of the eddy currents should be included in the solution.

***Index Terms*—Eddy currents, ferromagnetic materials, finite element methods, magnetic hysteresis, synchronous machines.**

I. Introduction

NUMERICAL field computation has long been a standard tool in the design and analysis of electrical machines. Radial-flux machines are commonly modeled with the 2-D finite element (FE) method providing sufficiently accurate estimates for the voltages, currents and torque which usually are the quantities of interest. Until today, however, accurate estimation of iron losses has been found relatively problematic and thus various different techniques for their modeling have been studied. The simplest models have been based on the statistical loss theory [1] applied in the postprocessing stage of the computation. More complicated postprocessing models have also been developed to take into account the rotation of the flux density [2] and to model the physical behavior of the eddy currents in the core laminations [3].

Besides the postprocessing models, significant effort has also been put into including the iron-loss effects into the field computation. Replacing the traditionally used single-valued (SV) material properties by a vector hysteresis model has been found relatively straightforward [4], [5]. The generally 3-D problem of the lamination eddy currents has been simplified by assuming the currents to flow only in the plane of the laminations and coupled to the 2-D field problem by several different methods. The simplest ones have neglected the skin effect of the eddy currents [6] or taken into account the phase lag between the average and surface fields by experimental formulas [7]. In more detailed approaches the skin effect and the flux-density distribution in the lamination have been modeled numerically [8]-[10].

Despite the variety of different loss models, only few publications could be found discussing the actual effects of the iron losses on the field solution. In [4], the flux-density distributions in a transformer T-joint computed both with SV and hysteretic material properties were compared. In [11] the proposed iron-loss model for 3-D FEM was verified by means of the power balance, i.e. comparing the calculated iron loss to the input power increase due to the iron-loss effects. However, in both cases, the effect of including the iron losses on the overall performance of the studied devices wasn't clearly stated. In [12] it was found that in the case of induction machines, the global quantities such as the torques and currents of the machine are almost unaffected by the inclusion of the iron losses into the field computation. Only the iron loss itself was found to decrease slightly when taking the losses into account.

Based on the small amount of such studies, it may be concluded that the users of the postprocessing models rely on the assumption that the effects of the iron losses on the simulation results remain negligible. On the other hand, however, the developers of the more complicated loss models seem uninterested to study if they could obtain sufficient results also with simpler models and less computational burden. Finding this an interesting topic to study from the points of view of both accuracy and computation time, we contribute to this field in this paper by studying the iron-loss effects in frequency-converter supplied synchronous machines. Due to the direct-current (DC) excitation, no iron losses are expected in most parts of the rotors of synchronous motors and generators, and thus their poles are often stacked of 2-mm steel sheets to reduce manufacturing costs. On the pole surface, however, flux-density harmonics caused by the slot ripple and especially frequency-converter supply may induce significant eddy currents on the thick and highly-conducting laminations [13]. This makes the synchronous machine an interesting application when the effects of the iron losses on the field solution are to be studied.

Based on our experience, the two major disadvantages of including the iron losses into the 2-D FE solution of laminated-core electrical machines are

Manuscript received December 13, 2011. Corresponding author: P. Rasilo (e-mail: paavo.rasilo@aalto.fi).
Digital Object Identifier inserted by IEEE

1. Numerical solution of the skin-effect problem of the eddy currents in the lamination requires several times more degrees of freedom than traditional FE formulations neglecting the iron losses. Thus the size of the system matrix increases and/or the forming of the system equations becomes more expensive.
2. The hysteretic material properties may cause problems in the convergence of the nonlinear iteration.

Due to these problems, we will here study how accurately the skin effect in the lamination should be modeled and if it is possible to use well-convergent SV material characteristics during the computation. Thus we compare the differences between three different iron-loss models:

1. Full inclusion of the hysteresis, eddy-current and excess losses in the computation using the model presented in [10] (*coupled, hysteretic model*).
2. Eddy currents coupled to the field solution. Hysteretic and rate-dependent material properties neglected, and the related losses calculated only in the postprocessing stage (*coupled*, *single-valued model*).
3. Conventional 2-D FE analysis with all the iron-losses neglected from the solution and calculated only in the postprocessing stage (*uncoupled model*).

With these three models, numerous FE simulations are performed for 12.5-MW and 150-kVA wound-field synchronous machines in different loading conditions with typical frequency-converter voltage waveforms. Special attention is paid on the required accuracy of modeling the skin effect of the lamination eddy currents. As the worst-case scenario, the 150-kVA machine is studied with unbalanced grid supply. Based on the results, reasonable parameters for the iron-loss model are determined in order to have a balance between the accuracy and computation time.

II. Methods

A. Iron-Loss Model

Consider a ferromagnetic lamination with a thickness d and conductivity σ being exposed to a time-varying magnetic field. The magnetic flux density $\boldsymbol{b}$ and field strength $\boldsymbol{h}$ are assumed to be parallel to the lamination surface and perpendicular to the z-axis placed in the direction of the thickness. If the thickness of the lamination is small compared to its other dimensions, the return paths of the eddy currents flowing in the lamination can be neglected, and the behavior of the field is described by the diffusion equation

$$\frac{\partial^2 \boldsymbol{h}(z,t)}{\partial z^2} = \sigma \frac{\partial \boldsymbol{b}(z,t)}{\partial t}. \tag{1}$$

The constitutive material law, i.e. the $\boldsymbol{h}(\boldsymbol{b})$ relationship, is generally hysteretic and includes also a dynamic part corresponding to the local excess losses in the lamination:

$$\boldsymbol{h}(\boldsymbol{b}) = \underbrace{\sum_{i=1}^{N_\phi} h_{\mathrm{hy}}\left(\boldsymbol{b}\cdot\boldsymbol{u}_\phi\right)\boldsymbol{u}_\phi}_{\text{hysteretic part}} + \underbrace{\sqrt{\sigma G V_0 S}\left|\frac{\partial \boldsymbol{b}}{\partial t}\right|^{-0.5}\frac{\partial \boldsymbol{b}}{\partial t}}_{\text{excess part}}. \tag{2}$$

The hysteretic part is obtained from an inverted vector Preisach model [5] and the excess-loss model is discussed in [1], [6] and [10]. In the simulations with SV material properties, the hysteretic and rate-dependent material properties are replaced by a single-valued reluctivity ν:

$$\boldsymbol{h}(\boldsymbol{b}) = \nu\left(|\boldsymbol{b}|\right)\boldsymbol{b}. \tag{3}$$

A solution for (1) as a series expansion of the flux density distribution was originally presented in [14] and [15]. Following the approach of [10], the flux density distribution is expressed as a truncated cosine series with N_b terms:

$$\boldsymbol{b}(z,t) = \sum_{n=0}^{N_\mathrm{b}-1} \boldsymbol{b}_n(t)\alpha_n(z) \text{ with } \alpha_n(z) = \cos\left(2n\pi\frac{z}{d}\right). \tag{3}$$

The field strength obtained by substituting (3) into (1) does not satisfy identically the constitutive material law, which must be therefore expressed weakly with respect to basis functions $\alpha_n(z)$. This leads to a system of N_b equations from which the field strength on the lamination surface can be solved:

$$\begin{bmatrix} \boldsymbol{h}_\mathrm{s}(t) \\ 0 \\ \vdots \end{bmatrix} = \frac{1}{d}\int_{-d/2}^{d/2} \boldsymbol{h}(z,t)\begin{bmatrix} \alpha_0(z) \\ \alpha_1(z) \\ \vdots \end{bmatrix} dz + \sigma d^2 \boldsymbol{C}\frac{\partial}{\partial t}\begin{bmatrix} \boldsymbol{b}_0(t) \\ \boldsymbol{b}_1(t) \\ \vdots \end{bmatrix}. \tag{4}$$

Matrix $\boldsymbol{C}$ is constant and depends only on the selected function space. The system can be solved iteratively by applying the Newton-Raphson method and calculating the Jacobian matrix from the differential reluctivity [10].

If only the first basis function is considered (N_b = 1), the skin effect is neglected and the classical low-frequency approximation [6] for the eddy currents is obtained:

$$\boldsymbol{h}_\mathrm{s}(t) = \frac{1}{d}\int_{-d/2}^{d/2} \boldsymbol{h}(z,t)\,dz + \frac{\sigma d^2}{12}\frac{\partial}{\partial t}\boldsymbol{b}_0(t). \tag{5}$$

Once the flux-density distribution in the lamination has been solved, the hysteresis, eddy-current and excess-loss densities are calculated locally in the lamination, integrated over the thickness and averaged over one period of supply. More details on the loss computation can be found in [10].

B. Electrical Machine Model

The flux-density distribution of electrical machines is analyzed by the 2-D FE method, in which the Ampere's law in the cross-sectional xy-plane is solved weakly with respect to nodal shape functions N_i. The flux linkages of the windings are imposed by the average flux-density component $\boldsymbol{B}_0$ (capital letters are used to denote the 2-D quantities), and thus the torque, voltages and currents of the machine depend on its distribution and time variation in the cross-sectional domain. To study the effect of the iron losses on the operation of the machine, the average flux density component needs to be solved both when coupling and not coupling the iron-loss effects to the solution.

To include the iron losses into the 2-D finite element method, the flux-density components $\boldsymbol{B}_n(x,y)$ in the laminated

$$\underbrace{\begin{bmatrix} \int_{\Omega_{\mathrm{Fe}}} \boldsymbol{D}^{\mathrm{T}} \frac{1}{d} \int_{-d/2}^{d/2} \boldsymbol{H}\left(\boldsymbol{a}_0,\ldots,\boldsymbol{a}_{N_\mathrm{b}-1}\right)\alpha_0 dz d\Omega \\ \int_{\Omega_{\mathrm{Fe}}} \boldsymbol{D}^{\mathrm{T}} \frac{1}{d} \int_{-d/2}^{d/2} \boldsymbol{H}\left(\boldsymbol{a}_0,\ldots,\boldsymbol{a}_{N_\mathrm{b}-1}\right)\alpha_1 dz d\Omega \\ \vdots \end{bmatrix}}_{\text{static and nonlinear part}} + \frac{1}{\Delta t}\underbrace{\begin{bmatrix} \int_{\Omega_{\mathrm{Fe}}} \boldsymbol{D}^{\mathrm{T}}\sigma d^2 \sum_{n=0}^{N_\mathrm{b}-1} C_{0n}\boldsymbol{D}\boldsymbol{a}_n d\Omega \\ \int_{\Omega_{\mathrm{Fe}}} \boldsymbol{D}^{\mathrm{T}}\sigma d^2 \sum_{n=0}^{N_\mathrm{b}-1} C_{1n}\boldsymbol{D}\boldsymbol{a}_n d\Omega \\ \vdots \end{bmatrix}}_{\text{dynamic part (current time step)}} = \frac{1}{\Delta t}\underbrace{\begin{bmatrix} \int_{\Omega_{\mathrm{Fe}}} \boldsymbol{D}^{\mathrm{T}}\sigma d^2 \sum_{n=0}^{N_\mathrm{b}-1} C_{0n}\boldsymbol{D}\boldsymbol{a}_n^{\mathrm{p}} d\Omega \\ \int_{\Omega_{\mathrm{Fe}}} \boldsymbol{D}^{\mathrm{T}}\sigma d^2 \sum_{n=0}^{N_\mathrm{b}-1} C_{1n}\boldsymbol{D}\boldsymbol{a}_n^{\mathrm{p}} d\Omega \\ \vdots \end{bmatrix}}_{\text{dynamic part (previous time step)}} \quad (6)$$

regions Ω_{Fe} are expressed as curls of corresponding vector-potential components $\boldsymbol{A}_n = A_n(x,y)\boldsymbol{u}_z$ [10]. The Ampere's law is applied to the surface field strength, and for symmetry reasons also to the other equations of system (4). The backward Euler time-discretization method with a time-step length of Δt is also employed. The discrete system of equations in the laminated regions is given in (6), in which $\boldsymbol{D}$ is the discrete $2\times N$ curl matrix, N being the number of shape functions in the 2-D domain and $\boldsymbol{a}_n$, $n = 0,\ldots,N_\mathrm{b}-1$ denote the vectors of nodal values of vector potentials A_n. The size of the total system matrix is $N_\mathrm{b}N\times N_\mathrm{b}N$. From now on, this model with full coupling of the eddy currents to the average flux density will be referred to as the *coupled model*.

The traditional 2-D FE formulation with iron losses neglected (*uncoupled model*) is used as a reference against which results from the *coupled model* are compared. The material properties are assumed to be single-valued and rate-independent with a reluctivity ν, and the eddy currents are not coupled to the average flux density to be solved. This leads to the traditional discrete weak form of Ampere's law for lossless iron:

$$\boldsymbol{S}(\boldsymbol{a}_0)\boldsymbol{a}_0 = \boldsymbol{0}\text{, with } S_{ij} = \int_{\Omega_{\mathrm{Fe}}} \nu(\boldsymbol{B}_0)(\nabla N_i)\cdot(\nabla N_j)\,d\Omega\,. \quad (8)$$

Basically only (8) is required to model the iron regions in the *uncoupled model*. However, we want to calculate the iron losses in exactly the same way as was done in the *coupled model* and thus only the first N equations of (6) are replaced by (8) and the rest of the equations are kept unchanged. In such way the average flux density is not affected by the iron-loss effects but the loss itself is calculated similarly to the *coupled model*. This is essential to compare the effects of the coupling on the iron loss itself. Otherwise any other postprocessing model could be applied as well.

III. Application and Results

A. Studied Machines

Two different wound-field synchronous machines are considered. Machine I is a 12.5-MW synchronous motor for a variable-speed extruder application. Machine II is a 150-kVA low-voltage synchronous generator for an industrial diesel-generator application. The FE meshes and essential data and dimensions of the two machines are shown in Fig. 1 and Table I, respectively.

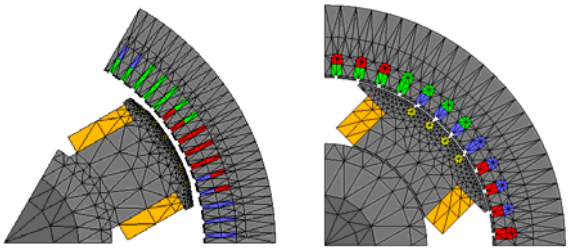

a) b)

Fig. 1 Finite element meshes of a) Machine I and b) Machine II. The two meshes are in different scales.

TABLE I
DATA AND DIMENSIONS OF THE MACHINES

Data	Machine I	Machine II
Machine type	motor	generator
Power	12500 kW	150 kVA
Voltage	3150 V	400 V
Current	2291 A	217 A
Displacement factor	1	0.8 cap
Frequency	50 Hz	50 Hz
Connection	star	star
Number of pole pairs	3	2
Stator outer diameter	1820 mm	430 mm
Stator inner diameter	1340 mm	300 mm
Air gap	15 mm	1.2 mm
Number of stator slots	90	48
Stator lamination	0.5-mm, 3.0-MS/m Fe-Si sheet	
Rotor lamination	2-mm, 7.9-MS/m steel sheet	

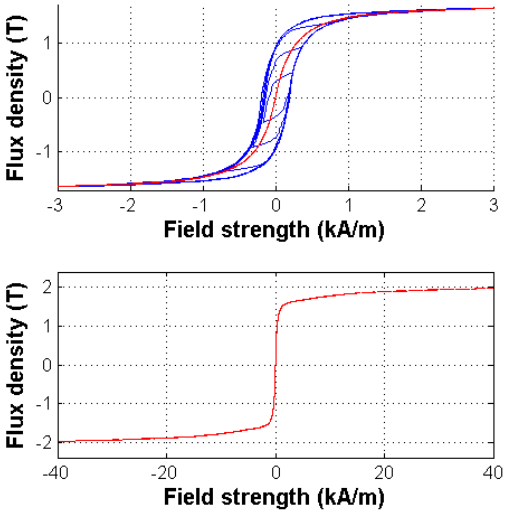

Fig. 2 Hysteretic and single-valued B-H curves used for the materials. The curves meet at full saturation

The stators of the machines are stacked of 0.5-mm Fe-Si electrical steel sheets while the rotor poles are made of 2-mm steel plates. Measured conductivities for the core materials are listed in the end of Table I. The two materials are assumed to have identical magnetization properties, i.e. the hysteresis curve shown in Fig. 2, which has been measured for the 2-mm steel plate. In reality, the B-H loop of the stator Fe-Si sheet is slightly steeper and narrower with over 60 % smaller static hysteresis loss than that of the steel plate, but convergence problems prevented the use of this curve in the iron loss model with more than two skin-effect terms. However, in order to study the worst-case effects of the hysteresis loss on the field solution, it is reasonable to use the curve with higher losses. $N_\phi = 4$ directions were used in the vector hysteresis model, and the scalar B-H loop applied in each direction was modified so that the vector model (2) produced the measured loop as output when supplied with a unidirectionally varying flux density.

The SV curve used for the *uncoupled model* is also shown in Fig. 2. The SV curve was obtained by averaging the field strengths of the lower and higher branches of the minor loop and gradually approaching the lower branch as the flux density increases up to the saturation value of 1.603 T. The excess-loss coefficients of (2) for the stator and rotor sheets were estimated by scaling the value $(\sigma G V_0 S)^{1/2} = 0.732$ $(\mathrm{W/m^3})(\mathrm{s/T})^{3/2}$ obtained for a 3.12-MS/m sheet in [10] by the ratio of the square roots of the conductivities.

B. Verification of the Iron-Loss Model

The iron-loss model has been verified by comparison to experimental core losses obtained by calorimetric measurements [16] for Machine II at no-load operation with open stator terminals. In the simulations, the machines were forced to rotate at the rated speed, the terminal current was set to zero and the field windings were supplied from a DC voltage source. 2000 time steps were used per one 50-Hz period and two periods were simulated in total to reach a steady state. Second-order FEs and $N_\mathrm{b} = 2$ skin-effect terms were used in the simulations. To allow using the actual B-H loop also for the stator sheet, SV material properties were assumed during the simulations while calculating the hysteresis and excess losses at the postprocessing stage. Due to differences between the measured and modeled losses, it was also found necessary to include the steel frame around the stator core into the FE model when the machine was simulated at voltages above the rated voltage. This can be seen in Fig. 3 in which the simulated and measured core losses are compared at different voltages. When the machine is highly saturated, a significant proportion of the flux is forced into the frame in which high eddy-current losses thus occur. Since the conductivity of the frame is not known accurately, and the end-shield effects are neglected in the 2-D model, the accuracy of the simulated frame loss cannot be guaranteed. However, since the simulated results are close to the measured ones, and the iron losses account for at least two thirds of the total core loss, the iron-loss model is concluded to work reasonably well to be used in the simulations of this paper.

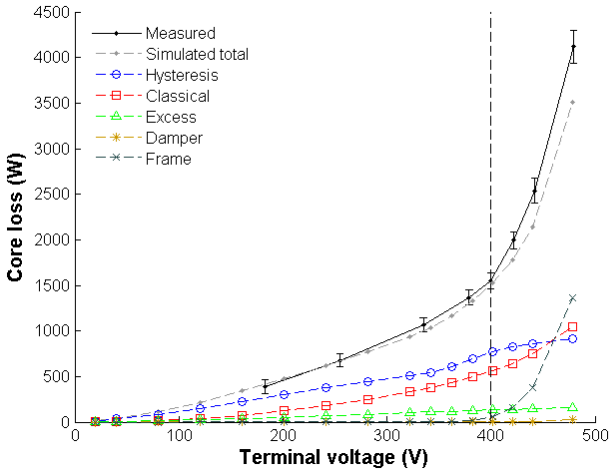

Fig. 3 Verification of the iron-loss model by comparison of measured and simulated no-load core losses for Machine II.

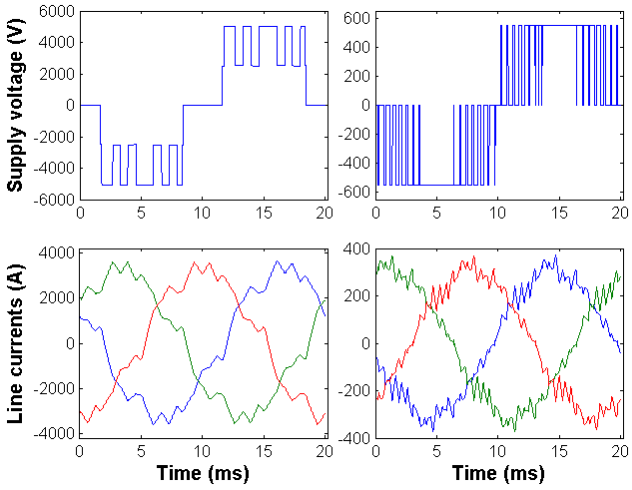

Fig. 4 One of the line-to-line voltages and the simulated rated-load currents of a) Machine I with DTC and b) Machine II with PWM supply.

C. FE Simulations with the Iron-Loss Models

The two machines were studied in seven different loading conditions ranging from no load up to 20 % overload operation. In all the loading conditions, the machines were operated at the rated displacement factors. Second-order elements were used and two 50-Hz periods were simulated using 3000 time steps per each period. Initial states for the time-stepping simulations were obtained by using a static FE solution coupled to an analytical two-axis synchronous-machine model, and iteratively changing the field voltage and rotor angle until the desired terminal power and displacement factor were reached. The time-stepping simulations were performed by forcing the machines to run at the synchronous speed and supplying the stator and field windings from voltage sources keeping the field voltage constant in the initial value. Machine I is designed for a direct-torque controlled (DTC) drive and thus a voltage waveform measured at the rated-load operation was used as the stator voltage for the simulations. Machine II was studied with a pulse-width modulated (PWM) voltage supply with a typical switching frequency of 2 kHz.

The supply voltages and the corresponding rated-load currents obtained with the *coupled model* are shown in Fig. 4. Since the iron losses were neglected from the static FE solutions, the initial states and voltages remained constant for all the three different iron-loss models studied within the time-stepping simulations.

In each operating point the machines were simulated with the *coupled model* using both hysteretic and single-valued material characteristics. In addition, the simulations were done with the *uncoupled model* using hysteretic material properties in the solution of the higher-order skin-effect terms but only SV materials for the average flux density. In each case, the number of skin-effect basis functions was varied in the range of $N_b = 1,\ldots,5$. Thus $7\times3\times5 = 105$ simulations were performed in total for each machine.

D. Power Balance

The power balance is a good tool to analyze the ability of the model to correctly include the iron losses into the field solution. Here, the power balance is defined as the relative error between the difference $P_{in} - P_{out}$ of the computed input and output powers, and the losses P_{loss} predicted by the model:

$$r = 1 - \frac{P_{loss}}{P_{in} - P_{out}}. \qquad (9)$$

The losses P_{loss} must comprise only those loss components which are included in the field solution. Thus, if the *SV model* is used, the hysteresis losses have to be left out from the equation. Similarly all the iron losses have to be neglected if the *uncoupled model* is used.

In the *SV* and *uncoupled models*, the errors (9) were found to be less than 2.5 % in all the 20-120 % loading points and in the no-load point of Machine I. In the no-load point of Machine II, errors of 8.2 % were obtained with the *uncoupled model* which implies some difficulties in the modeling the no-load operation with voltage supply. In both machines, the errors tend to decrease when the loading increases.

Errors up to 12.6 % were observed when the *coupled hysteretic model* was used. The errors have their maximums at $N_b = 2$ skin-effect terms in no-load operation but decrease when the number of skin-effect terms is increased. To minimize memory consumption during the computation, the hysteresis losses are calculated exactly in the same sample points that are used in the numerical integrations of (6), and thus the accuracy increases when more sample points are used along the lamination thickness. Nevertheless, the power balance is concluded to be satisfied reasonably well.

E. Influence on Core Losses

Fig. 5 shows the dependence of the core losses on the number of skin-effect basis functions at the rated-load operation. In addition, the dependence on the loading is shown in the case of $N_b = 4$ skin-effect terms. In both machines on the stator side, the core losses seem to be almost independent on the number of basis functions. Slight variation can nevertheless be seen in the hysteresis loss. On

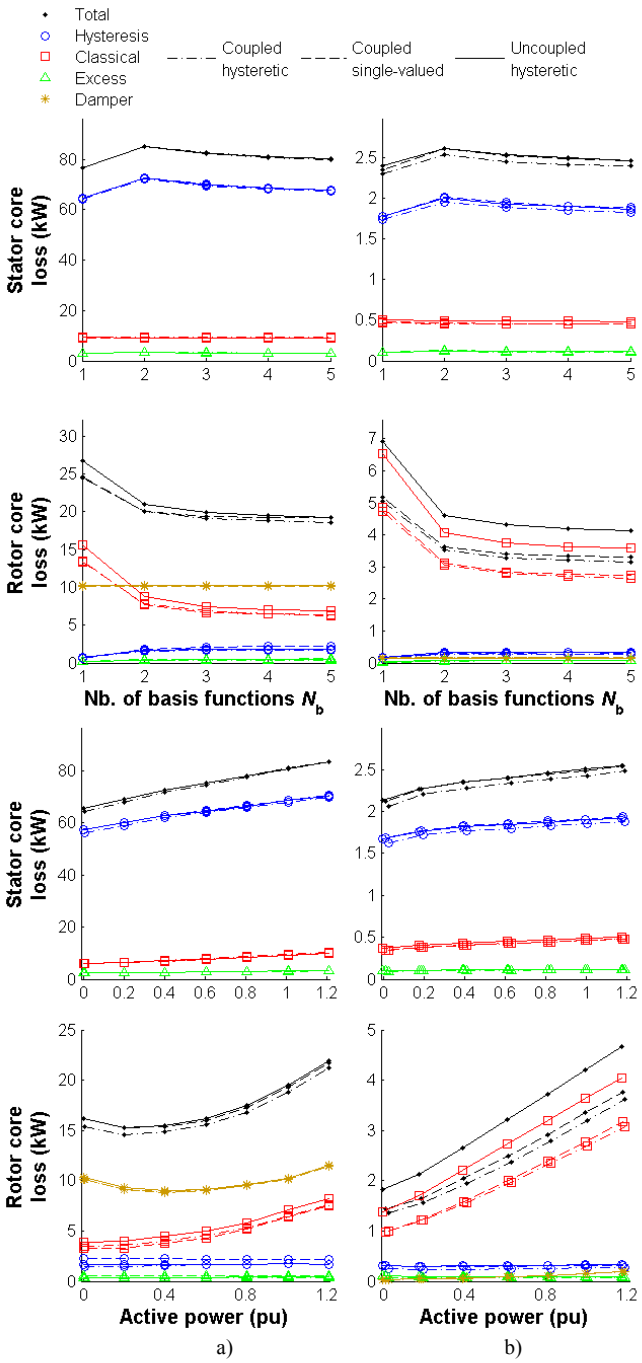

Fig. 5 Dependence of the core losses on the number of skin-effect basis functions at the rated load, and on the load with $N_b = 4$ skin-effect terms. a) Machine I and b) Machine II.

TABLE II
EFFECT OF SV MATERIALS AND UNCOUPLING ON THE CORE LOSSES RELATIVE TO THE COUPLED HYSTERETIC MODEL ($N_b = 4$)

Load (%)	Effect of SV materials (W)		Effect of uncoupling (W)	
	Machine I	Machine II	Machine I	Machine II
0	+1987 (+2.5 %)	+188 (+5.7 %)	+1901 (+2.4 %)	+523 (+16.0 %)
20	+1699 (+2.1 %)	+182 (+4.9 %)	+1696 (+2.1 %)	+694 (+18.7 %)
40	+1233 (+1.4 %)	+194 (+4.6 %)	+1274 (+1.5 %)	+834 (+19.9 %)
60	+881 (+1.0 %)	+201 (+4.3 %)	+993 (+1.1 %)	+953 (+20.4 %)
80	+852 (+0.9 %)	+213 (+4.1 %)	+936 (+1.0 %)	+1036 (+20.2 %)
100	+745 (+0.7 %)	+249 (+4.5 %)	+890 (+0.9 %)	+1130 (+20.3 %)
120	+701 (+0.7 %)	+241 (+4.0 %)	+806 (+0.8 %)	+1153 (+19.1 %)

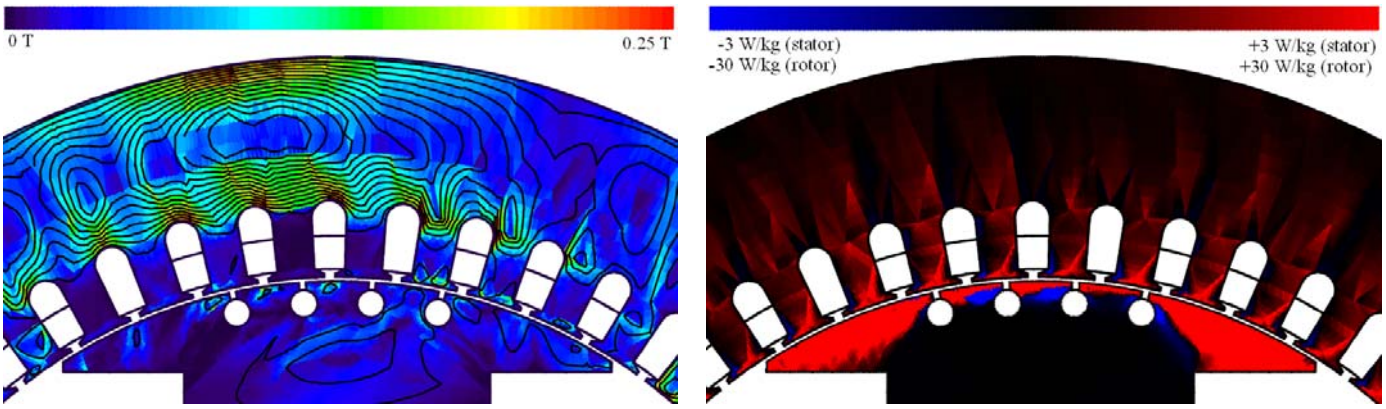

a) b)

Fig. 6 Differences in a) the instantaneous average flux density and b) the time-averaged core losses between the *uncoupled model* and the *coupled hysteretic model* in Machine II at 20-% overload operation with $N_b = 4$. Different scales are used in b) for the stator and the rotor. Direction of rotation is counterclockwise.

the rotor side, however, the eddy-current loss is reduced by 45–55 % when the number of basis functions is increased from 1 to 5. The hysteresis and excess losses are slightly increased, but their proportion on the total rotor loss is small. Depending on the load, the corresponding decrease in the total core loss is 2.5-3.6 % in Machine I and 24-38 % in Machine II. The difference between the two machines is explained by the fact that the rotor core loss comprises most of the total core loss in Machine II while the stator core loss is dominant in Machine I. As expected, accurate modeling of the skin effect is more essential on the rotor side due to the thick laminations and the high-frequency eddy currents induced on the pole surface.

In both machines, the iron losses increase with loading. Noticeable is that in Machine I, the DTC supply causes significant damper winding losses and that this loss is has its minimum at the 40-% load. The damper-winding losses are unaffected by the iron-loss model and the number of skin-effect basis functions. However, the iron losses seem to be overestimated by both the *SV model* and the *uncoupled model* in all the loading points when compared to the *coupled hysteretic model*. Table II compares the total core losses calculated with the *SV* and *uncoupled models* to the losses from the *coupled model* in case of the simulations with $N_b = 4$ skin-effect terms. Both the absolute and relative differences are shown.

In Machine I, uncoupling the eddy currents from the field solution changes the core losses very little compared to the case when SV materials are used. The differences between the models tend to decrease when the loading increases. On the contrary in Machine II, the effect of eddy currents overcomes the effect of the material properties, and the effect seems to increase with loading. Again, these observations are explained by the different distributions of the total iron losses between the stator and the rotor in the two machines. Indeed, the magnetic material characteristics seem to affect mainly the hysteresis losses while uncoupling the eddy currents mostly increases the eddy-current losses, which seems reasonable.

In Fig. 6, the flux-density and core-loss distributions of Machine II obtained with the *coupled model* are subtracted from those obtained with the *uncoupled model*. In the loss-density plot, the red regions correspond to the ones in which

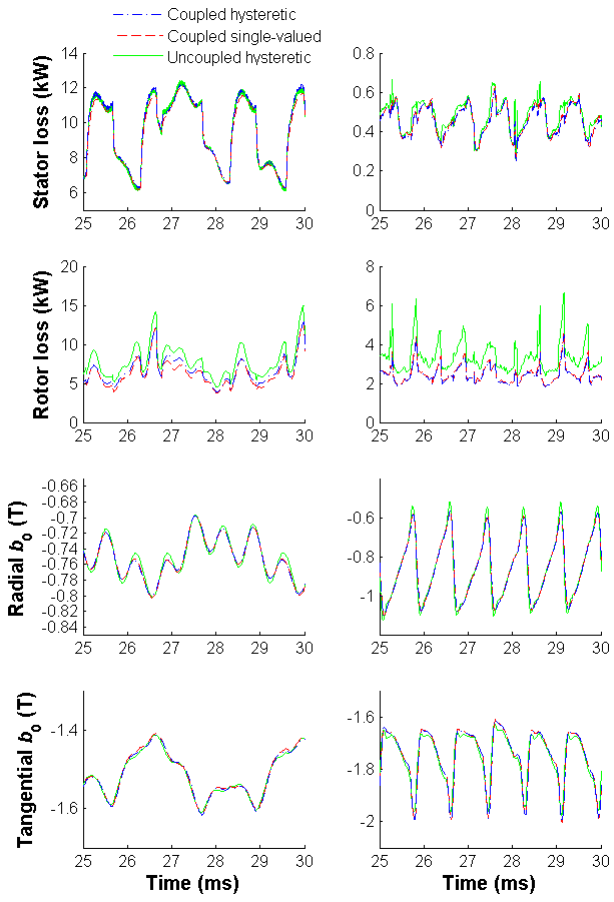

a) b)

Fig. 7 Stator and rotor eddy-current losses and the radial and tangential components of the average flux densities on the surface of the leading edge of the pole shoe at the rated-load operation with $N_b = 4$ in a) Machine I and b) Machine II.

this difference is positive. Although the instantaneous flux-density distribution seems to differ mostly on the stator side, the most significant differences in the losses occur on the rotor side. This implies that the iron losses cause the flux of the *coupled model* to lag that of the *uncoupled model*, but once the losses are averaged over a full period, no significant differences occur on the stator side. In the rotor, it can be seen that the *uncoupled model* gives higher losses in most parts of

the pole shoe. Since the eddy currents are induced by high-frequency flux harmonics, the related losses are inductance limited in nature. This means that in the *coupled model*, the reaction fields of the eddy currents have a damping effect on the inducing flux harmonics and thus prevent them from penetrating too deeply into the pole shoe. This reduces the loss when compared to the *uncoupled model*.

The previous observations are further supported by Fig. 7, which shows the instantaneous stator and rotor eddy-current losses as well as the radial and tangential flux-density components near the surface of the leading edge of the pole shoe for both machines at the rated-load operation. A slight phase difference can be seen in the time-variation of the stator eddy-current losses between the *coupled* and *uncoupled models*. On the rotor side, especially the radial flux-density components are increased in the *uncoupled model* due to the reduced damping effect, which causes the increase also in the eddy-current losses.

The observations that the iron losses increase if the coupling is removed and that this effect is much more significant for the smaller machine agree with the results of [12]. In this case, however, unambiguous conclusions cannot be drawn on the dependency of the overestimation on the loading conditions. This appears to be strongly dependent on the distribution of the iron losses between the stator and the rotor.

F. Influence on Operating Conditions

Despite the sensitivity of the no-load operating point of Machine II, the operating points of the machines at higher loads remain fairly constant independent of the loss model in use. In Machine I, the active terminal powers change less than 2 % at 20 % load and less than 0.3 % at higher loads when the model is changed from the *coupled* to the *uncoupled model*. In Machine II, the corresponding change decreases from 9.7 % at 20-% load to 1.4 % at overload. Fig. 8 visualizes the effect at the rated load also for the electromagnetic torque, fundamental component of the terminal current and displacement factor. Since the electrical operating point stays nearly constant and the power balance is satisfied reasonably, the effect of neglecting the iron losses from the field solution can be seen as the increase of the electromagnetic torque in case of Machine II. Again, the results are in correspondence with [12] which concluded that the inclusion of the iron losses in the field solution mainly affects the iron loss itself.

Although the fundamental components of the terminal currents remain almost unchangeable between the three studied models, it is possible that the harmonic contents are affected by the damping effect of the iron losses. Fig. 9 shows the relative effect of the iron-loss model on the total harmonic distortion (THD) contents of the terminal current and the electromagnetic torque. It can be seen that uncoupling the hysteresis and the eddy current losses from the field solution slightly reduces the harmonic contents of the terminal current due to increased inductance encountered by the flux of the machine. The effect is illustrated in Fig. 10 where the terminal current waveforms obtained with the *SV* and *uncoupled*

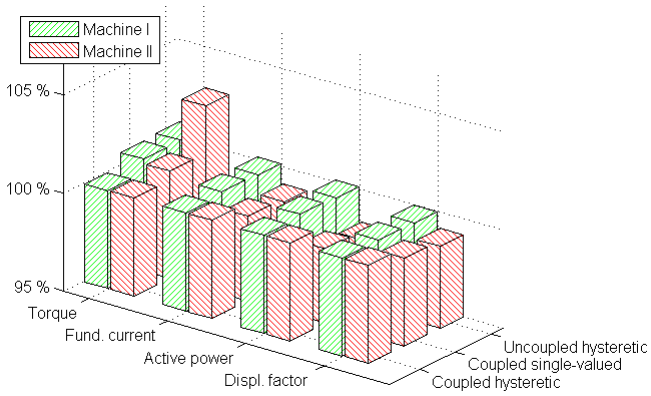

Fig. 8 Relative effect of the iron-loss model on some global quantities of the machines at the rated-load operation with $N_b = 4$ skin-effect terms.

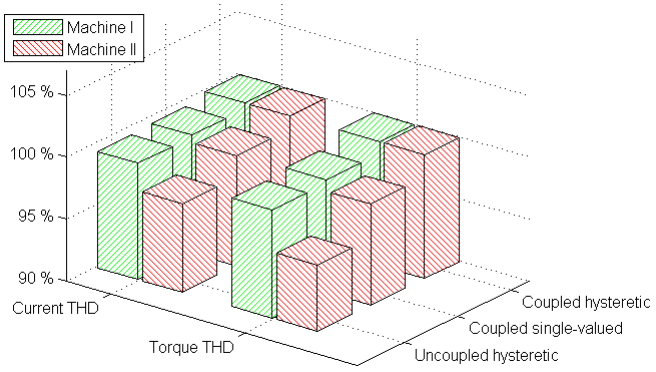

Fig. 9 Relative effect of the iron-loss model on the THD levels of the terminal current and the electromagnetic torque at the rated-load operation with $N_b = 4$ skin-effect terms. Note that the order of the models differs from that of Fig. 8.

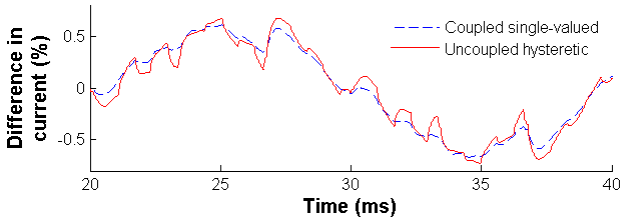

a)

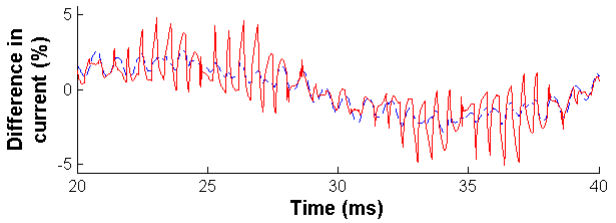

b)

Fig. 10 Differences in the terminal currents of a) Machine I and b) Machine II between the *coupled hysteretic model* and the *SV* and *uncoupled models* at the rated-load operation with $N_b = 4$. The differences are calculated relative to the effective value of the current from the *coupled hysteretic model*.

models are subtracted from the waveforms obtained with the *coupled model* (i.e. the ones shown in Fig. 4). It can be seen that the difference in the high-frequency contents is greater between the *uncoupled model* and the *coupled model* than between the *SV model* and the *coupled model*. The differences are shown relative to the effective values of the *coupled-model*

currents. The THD change caused by the uncoupling is less than 0.5 % for Machine I and less than 3 % for Machine II.

The harmonic contents of the torque are almost unaffected by the iron-loss model. However, the relative THD is reduced due to the increased average torque when the iron losses are uncoupled from the field solution.

G. Effect of Inverter Waveform

To ensure that the differences in the iron-loss effects between the two machines were not caused by the different supply-voltage waveforms, the simulations for Machine I were repeated using the same 2-kHz PWM supply as earlier for Machine II. The effects of the SV materials and uncoupling the iron losses were found to be 0.7-3.0 % and 1.0-3.2 %, respectively. The slight increase to the values of Table II is mostly caused by the reduction of the damper-winding losses to approximately half of their original value. Compared to the DTC supply, the iron losses are reduced by 1-8 %, slightly more in the *coupled model* than in the other models. Either way, the differences between the *coupled model* and the *SV* and *uncoupled models* remain smaller than those in Machine II.

H. Effect of Unbalance

Unbalanced operating conditions impose extra harmonics into the rotating magnetic fields of electrical machines, which leads to a subsequent increase in the core losses. In grid-supplied synchronous machines, the most common source of unbalance are asymmetric line currents resulting from unbalanced voltages or asymmetric loading, which impose backward-rotating components into the flux of the machine [17]. On the rotor side, these components are seen as harmonics with frequencies ranging up from double supply frequency which makes the unbalanced operation an interesting special case considering the topic of this paper.

To assess the influence of the unbalance, Machine II was simulated in the rated-load operation with sinusoidal voltage supply including a backward-rotating voltage component with a magnitude of 30 % of the forward-rotating one. Comparing this value to the steady-state limitation of 1 % set by standard [18], the case is highly exaggerated and easily covers the realistic worst-case scenarios at least in steady-state operation. Thus, the study is expected to bring out any possible effects of the iron losses on the field solution which were not observed with the balanced PWM supply.

Fig. 11 shows the unbalanced line-to-line voltages and the resulting currents obtained with the *coupled model* with $N_b = 4$ skin-effect terms. Fig. 12 segregates the core losses and shows the global quantities obtained with the three iron-loss models. It is seen that although the supply voltages are sinusoidal, the unbalance causes the rotor eddy-current losses to increase close to the same level as with the PWM supply. The damper-winding losses are over 20 times higher than in the previous case. However, the differences in the core losses between the three models seem to be very similar to those shown in Fig. 5. Also the torque behaves similarly to the previous cases. The fundamental current, active power and total power factor vary less than 1.3 % between the three models.

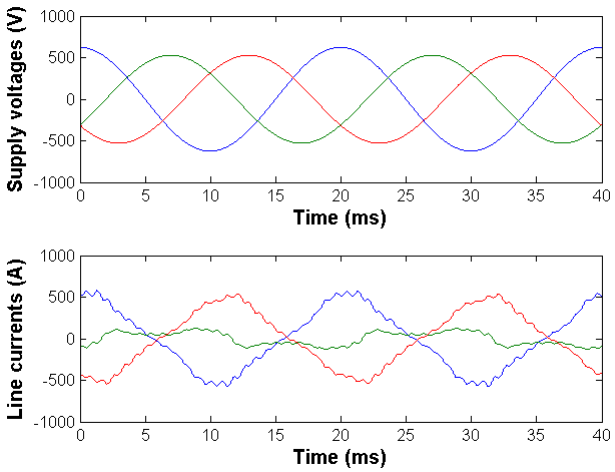

Fig. 11 Unbalanced voltages and simulated line currents of Machine II.

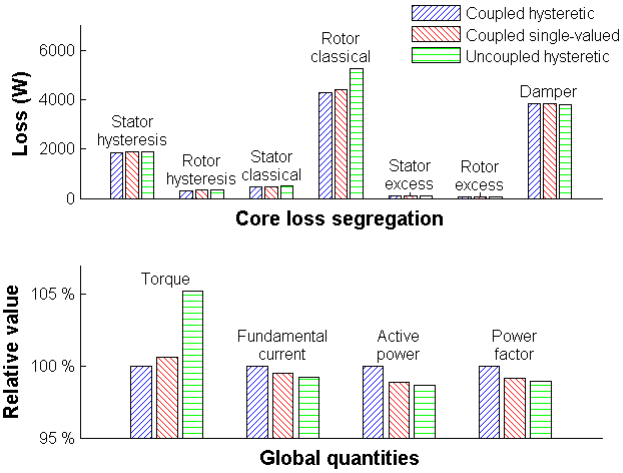

Fig. 12 Differences in the results between the three models ($N_b = 4$) in Machine II supplied with unbalanced network voltages.

I. Computation Time

Increasing the number of skin effect terms also increases the size of the system matrix. The total number of equations in the FE model is

$$N_{eq} = N_{tot} + (N_b - 1)N + N_{circ}, \qquad (10)$$

in which N_{tot} is the total number of nodes, N is the number of nodes in the laminated regions and N_{circ} is the number of circuit equations. These data for the two machines are shown in Table III.

The average computation time per time step and the required number of Newton-Raphson iterations as a function of the number of skin-effect basis functions are shown in Fig. 13 for the rated-load simulations. For both machines, the computations with the hysteretic material properties took 2.5-3 times longer than those with the SV materials. With hysteretic materials, the computation of Machine I took slightly longer due to higher number of system equations. However, with the single-valued material characteristics, the computation of Machine II took longer due to higher level of saturation.

IV. Conclusion

Effects of iron-loss modeling on the finite element simulation of wound-field synchronous machines were studied. Despite the high-conductivity and thick rotor laminations commonly used as the construction material of synchronous machines, it was found that inclusion of the iron losses into the field solution does not significantly affect the electrical operating points, i.e. the terminal currents or displacement factors. When the iron losses were uncoupled from the field solution, the harmonic contents of the stator current slightly decreased due to increased inductances encountered by the flux of the machine. In addition, the mean value of the electromagnetic torque increased in the motoring mode of operation due to decreased loss power included in the field solution. Otherwise, the inclusion of the iron losses was mainly found to affect the iron loss itself.

Based on the presented results, it is concluded that in the 150-kVA machine, incorporating the eddy-current losses into the field computation is important in order to accurately predict the core losses and the electromagnetic torque. Indeed, depending on the load, uncoupling the eddy-current losses from the field solution resulted into a 16-20 % overestimation in the total core losses when compared to the *coupled model*. If the eddy currents were included, but single-valued material characteristics were used instead of the hysteresis model, the overestimation was less than 4.9 % at loads of 20 % and higher.

In the 12.5-MW machine, both effects were less significant. When single-valued materials were used, the overestimation of the core losses was less than 2.5 % in all the studied loading points. In addition, uncoupling the eddy currents from the solution only caused an additional increase of less than 0.1 percentage points when compared to the simulation with single-valued materials. Thus the material characteristics have a relatively bigger effect on the field solution in the larger machine than in the smaller one. This is explained by the higher proportion of the stator losses on the total core losses in the larger machine. However, it is emphasized that if the rotor core losses are to be segregated from the total core losses, the eddy currents play a more significant role and 3 to 5 skin-effect terms should be used in the applied loss model for both machines to accurately model the corresponding losses on the rotor side.

Unbalanced voltage supply of the 150-kVA machine was studied as a possible worst-case scenario on the effects of the iron losses on the FE solution. Also in this case, where the backward-rotating flux induces high-frequency eddy currents into the rotor, the effects of the iron-loss model on the electrical operating point remain almost negligible. The most significant overestimation was again observed in the eddy-current losses on the rotor side predicted by the uncoupled model.

In both studied machines, the effect of the hysteretic material properties on the computed core loss and global quantities can be considered fairly insignificant. Considering the commonly-recognized difficulties related to hysteresis modeling, as well as the possibilities of reducing computation time, it can be seen reasonable to neglect the hysteresis losses from the field solution and to calculate the related losses only at the postprocessing stage.

TABLE III
NUMBERS OF ELEMENTS, NODES AND CIRCUIT EQUATIONS

Machine	Elements in total	Nodes in total N_{tot}	Nodes in iron N	Circuit equations N_{circ}
Machine I	2266	5327	2423	10
Machine II	1622	3667	2007	8

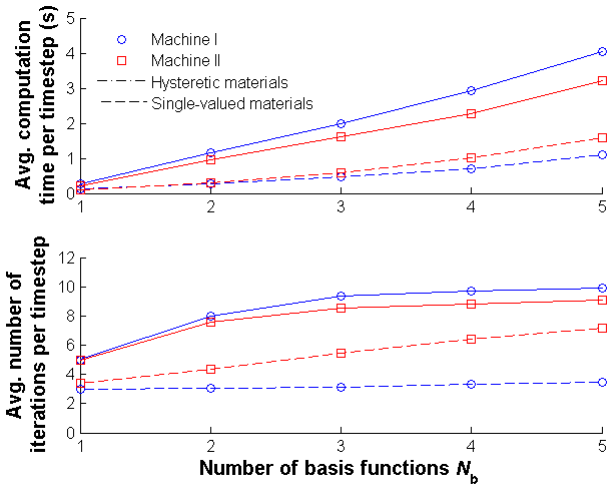

Fig. 13 Average computation time and average number of Newton-Raphson iterations per time step in the rated-load simulations.

Acknowledgment

Paavo Rasilo thanks the Academy of Finland, the Fortum foundation, the Finnish Foundation for Economic and Technical Sciences (KAUTE), the Walter Ahlström foundation and the foundation of the Association of Electrical Engineers in Finland (Sähköinsinööriliiton Säätiö) for financial support. Dr. Emad Dlala is acknowledged for originally implementing the hysteresis model.

References

[1] G. Bertotti, "General Properties of Power Losses in Soft Ferromagnetic Materials," *IEEE Trans. Magn.*, Vol. 24, No. 1, pp. 621-630, January 1988.

[2] A. Belahcen, A. Arkkio, "Comprehensive Dynamic Loss Model of Electrical Steel Applied to FE Simulation of Electrical Machines," *IEEE Trans. Magn.*, Vol. 44, No. 6, pp. 886-889, June 2008.

[3] K. Yamazaki, N. Fukushima, "Iron Loss Model for Rotating Machines Using Direct Eddy Current Analysis in Electrical Steel Sheets," *IEEE Trans. Energy Convers.*, Vol. 25, No. 3, pp. 633-641, September 2010.

[4] L. R. Dupré, J. J. Gyselinck, J. A. Melkebeek, "Complementary Finite Element Methods in 2D Magnetics Taking Into Account a Vector Preisach Model," *IEEE Trans. Magn.*, Vol. 34, No. 5, pp. 3048-3051, September 1998.

[5] E. Dlala, J. Saitz, A. Arkkio, "Inverted and Forward Preisach Models for Numerical Analysis of Electromagnetic Field Problems," *IEEE Trans. Magn.*, Vol. 42, No. 8, pp. 1963-1973, August 2006.

[6] L. A. Righi, N. Sadowski, R. Carlson, J. P. A. Bastos, N. J. Batistiela, "A New Approach for Iron Losses Calculation in Voltage Fed Time Stepping Simulations," *IEEE Trans. Magn.*, Vol. 37, No. 5, pp. 3353-3356, September 2001.

[7] E. Dlala, A. Belahcen, A. Arkkio, "Simplified Iron Loss Model for Laminated Magnetic Cores" *IEEE Trans. Magn.*, Vol. 44, No. 11, pp. 3169-3172, November 2008.

[8] O. Bottauscio, M. Chiampi, "Analysis of Laminated Cores Through a Directly Coupled 2-D/1-D Electromagnetic Field Formulation," *IEEE Trans. Magn.*, Vol. 38, No. 5, pp. 2358-2360, September 2002.
[9] E. Dlala, A. Belahcen, A. Arkkio, "Efficient magnetodynamic lamination model for two-dimensional field simulation of rotating electrical machines," *J. Magn. Magn. Mater.*, Vol. 320, No. 20, pp. 1006-1010, October 2008.
[10] P. Rasilo, E. Dlala, K. Fonteyn, J. Pippuri, A. Belahcen, A. Arkkio, "Model of Laminated Ferromagnetic Cores for Loss Prediction in Electrical Machines," *IET Electr. Power Appl.*, Vol. 5, No. 7, pp. 580-588, August 2011.
[11] D. Lin, P. Zhou, Q. M. Chen, N. Lambert, Z. J. Cendes, "The Effects of Steel Lamination Core Losses on 3D Transient Magnetic Fields," *IEEE Trans. Magn.*, Vol. 46, No. 8, pp. 3539-3542, August 2010.
[12] E. Dlala, "On the Importance of Incorporating Iron Losses in the Magnetic Field Solution of Electrical Machines," *IEEE Trans. Magn*., Vol. 46, No. 8, pp. 3101-3104, August 2010.
[13] P. Rasilo, A. Arkkio, "Modeling the Effect of Inverter Supply on Eddy-Current Losses on Synchronous Machines," SPEEDAM, Pisa, Italy, June 2010.
[14] J. Gyselinck, R. V. Sabariego, P. Dular, "A Nonlinear Time-Domain Homogenization Technique for Laminated Iron Cores in Three-Dimensional Finite-Element Models," *IEEE Trans. Magn.*, Vol. 42, No. 4, pp. 763-766, April 2006.
[15] P. Dular, "A time-domain homogenization technique for lamination stacks in dual finite element formulations," *J. Comp. Appl. Math.*, Vol. 215, pp. 390-399, May 2008.
[16] P. Rasilo, J. Ekström, A. Haavisto, A. Belahcen. A. Arkkio, "Calorimetric System for Measurement of Synchronous Machine Losses," accepted for publication in *IET Electr. Power Appl.*, 2012.
[17] I. D. Mayergoyz, F. P. Emad, M. A. Sherif, "Electromagnetic field analysis of unbalanced regimes of synchronous machines," *J. Appl. Phys.*, Vol. 63, No. 8, pp. 3188-3190, April 1988.
[18] IEC 60034-1, "Rotating Electrical Machines – Part 1: Rating and Performance," 11th Edition, April 2004.

Paavo Rasilo was born in Äänekoski, Finland, in 1983. He received his M.Sc. (Tech.) in Electrical Engineering from Helsinki University of Technology (currently Aalto University), Espoo, Finland in 2008. He is currently working towards the Ph.D. degree in the Department of Electrical Engineering in Aalto University School of Electrical Engineering. His research is related to modeling and measurement of power losses in frequency-converter supplied synchronous machines.

Anouar Belahcen was born in Essaouira, Morocco, in 1963. He received the B.Sc. degree in physics (Licence es-science) from the University Sidi Mohamed Ben Abdellah, Fes, Morocco, in 1988 and the M.Sc. (Tech.), LisTech, and Doctorate degrees from Helsinki University of Technology, Helsinki, Finland, in 1998, 2000, and 2004, respectively.

From 1996 to 1998, he was a Research Assistant at the Laboratory of Electromechanics, Helsinki University of Technology. From 1998 to 2004, he was a Research Scientist and from 2004 to 2008 he was a Senior Researcher at the same Laboratory. Since 2008, he has been working as an Adjunct Professor in the field of coupled problems and material modeling at the Department of Electrical Engineering, School of Electrical Engineering, Aalto University, Espoo, Finland. His research interests deal with the numerical modeling of electrical machines, especially magnetic material modeling, coupled magnetic and mechanical problems, magnetic forces, and magnetostriction.

Antero Arkkio was born in Vehkalahti, Finland in 1955. He received his M.Sc. (Tech.) and D.Sc. (Tech.) degrees from Helsinki University of Technology in 1980 and 1988. Currently he is a Professor of Electrical Engineering at Aalto University. His research interests deal with modeling, design, and measurement of electrical machines.